Polarized laser excitation, electron paramagnetic resonance, and crystal-field analyses of Sm^{3+}-doped $LiYF_4$

J.-P. R. Wells
Optical Materials Research Center, Department of Physics and Applied Physics, University of Strathclyde, Glasgow G1 1XN, Scotland, United Kingdom

M. Yamaga
Department of Electronics, Faculty of Engineering, Gifu University, Gifu 501-1193, Japan

T. P. J. Han and H. G. Gallagher
Optical Materials Research Center, Department of Physics and Applied Physics, University of Strathclyde, Glasgow G1 1XN, Scotland, United Kingdom

M. Honda
Department of Physics, Naruto University of Education, Naruto, Tokushima 772-8502, Japan
(Received 11 February 1999; revised manuscript received 30 April 1999)

Using both optical absorption and laser-excited fluorescence, we have determined 55 crystal-field energy levels of the Sm^{3+} center in $LiYF_4$:Sm^{3+}. Electron paramagnetic resonance determines the symmetry of the center to be tetragonal, with effective spin Hamiltonian parameters of $g_{\|}=0.410\pm0.005$ and $g_{\perp}=0.644\pm0.002$. Inclusion of hyperfine interactions yields magnetic hyperfine constants of $A_{\|}=205\pm5$ MHz and $A_{\perp}=735\pm5$ MHz for the ^{147}Sm isotope and $A_{\|}=165\pm5$ MHz and $A_{\perp}=605\pm5$ MHz for the ^{149}Sm isotope. Truncating the $4f^5$ configuration to the lowest 30 multiplets, D_{2d} symmetry crystal-field fits to the experimental energy levels yield physically reasonable crystal-field parameters with standard deviations under 11 cm^{-1}. Simultaneous diagonalization of the crystal- and magnetic-field perturbation matrices give calculated magnetic splitting factors in good agreement with the measured ground-state g factors. [S0163-1829(99)12929-1]

I. INTRODUCTION

$LiYF_4$ is a tetragonal fluoride crystal of the Scheelite structure. Hence it belongs to the C_{4h}^6 space group. This compound is favorable for the introduction of trivalent rare-earth ions as they substitute for the Y^{3+} ions and require no charge compensation. Each Y^{3+} ion is surrounded by a dodecahedron of eight F^- ions and, consequentially, has a point group symmetry of D_{2d}. In fact, there is a slight distortion of the F^- dodecahedron cage which reduces the symmetry at the Y^{3+} (and, hence, trivalent rare-earth) site to S_4. As the distortion angle is very small ($\sim$2.3°), many authors choose D_{2d} as a realistic approximation to the actual S_4 site symmetry.

Rare-earth (R^{3+}) doped $LiYF_4$ has been studied by many authors, largely motivated by the prospect of solid-state optical devices, e.g., Tonelli *et al.*[1] Esterowitz *et al.*[2] performed polarized absorption and fluorescence studies of $LiYF_4$:Pr^{3+}. A crystal-field analysis of this data provided basis functions for a Judd-Ofelt analysis of the spectral line intensities. It was concluded in this work that the absence of many transitions (expected to be allowed for electric dipole selection rules under S_4 symmetry) could be explained using the higher D_{2d} symmetry, for which these transitions are forbidden.

Similar studies have been performed on $LiYF_4$:Eu^{3+}.[3,4] Görller-Walrand *et al.*[5] have completed crystal-field fits to 120 crystal-field levels assuming S_4 symmetry for the Eu^{3+} ion center, based on polarized absorption measurements in the 4000–39 000 cm^{-1} range. Using this comprehensive basis set, Fluyt *et al.*[6] have completed a Judd-Ofelt analysis assuming D_{2d} symmetry, thereby reducing the number of parameters involved. Such intensity parametrizations have shown themselves to be useful tests of the validity of using the D_{2d} approximation to the actual S_4 symmetry.

R^{3+}-doped $LiYF_4$ has also been shown to be a useful host for studies of quantum upconversion. $LiYF_4$:Pr^{3+} has demonstrated efficient infrared-to-blue upconversion,[7,8] while $LiYF_4$:Tm^{3+} has displayed infrared-to-ultraviolet upconversion via a photon avalanche effect.[9] Indeed, upconversion lasing has been demonstrated using $LiYF_4$:Er^{3+},[10] $LiYF_4$:Nd^{3+},[11] and $LiYF_4$:Tm^{3+}.[12] Typically, such lasing is cw pumped and the output consists of a semirandom pulse train with a power-dependent repetition rate. Conversion efficiencies of up to 10% of the incident pump light have been obtained.

In this study, we present optical absorption, laser excitation, and polarized fluorescence spectra of $LiYF_4$:Sm^{3+}. $LiYF_4$ is a particularly convenient host for studying Sm^{3+} because its substitution for a trivalent ion prevents the coexistence of the divalent species for which one cannot easily perform ''ion-selective'' spectroscopy in a conventional manner. This is because the strong $4f\rightarrow4f^{N-1}5d$ transitions are broad and overlapping as is the case in fluorite crystals where the samarium ion substitutes for the divalent cation.[13] For the fluorescence spectra presented in this work, we choose a comparatively low dopant concentration to avoid

Sm^{3+}-Sm^{3+} ion coupling as has been observed in other host crystals. This results in strong cross-relaxation processes which have been shown to quench the $^4G_{5/2}$ optical excitation.[14–16] Electron paramagnetic resonance (EPR) has been used to unambiguously determine the site symmetry of the single Sm^{3+} center present in $LiYF_4$:0.1% Sm^{3+} crystals as having tetragonal symmetry. In addition, these resonances show structure due to hyperfine interactions between the Kramers conjugate ground states of the ^{147}Sm and ^{149}Sm isotopes with nonzero nuclear spin. Experimental determination of the $4f$ wave function symmetries (from polarized laser excited fluorescence) has provided the basis for comprehensive crystal-field fits to the 55 measured Sm^{3+} energy levels assuming D_{2d} symmetry with good agreement between theory and experiment. These crystal-field fits allow calculation of the g values measured in the EPR experiments.

II. CRYSTAL GROWTH

The $LiYF_4$:Sm^{3+} crystals were grown by the Bridgman-Stockbarger technique using a furnace design originally developed for the growth of simple fluorides.[17] Oxygen is removed from the furnace using a rotary pump combined with a small diffusion pump, and then the chamber is filled with purified argon gas to a pressure slightly greater than 1 atm to minimize evaporative losses. The graphite crucible used in all runs has dimensions 15 mm internal diameter by 100 mm long with a 1° internal taper and a cone angle of 30°. $LiYF_4$ is incongruently melting at a temperature of 819 °C with a composition of 49 mol % YF_3 and 51 mol % LiF.[2] The slight excess of LiF ensures nucleation and growth of doped crystals under the desired phase. In order to avoid constitutional supercooling, the crystals were grown in a temperature gradient of 40 °C/cm with a translation rate of 0.8 mm/h. In these unseeded growth runs, the as grown crystal boules are randomly oriented and oriented spectroscopic samples were prepared using Laue x-ray-diffraction photography.

III. EXPERIMENTAL DETAILS

Optical absorption spectra in the visible range were measured at 10 K using Cary-AVIV double-beam spectrophotometer with a CTI-Cryogenics model 22C cold cycle refrigeration unit. Infrared absorption spectra were obtained at a sample temperature of 10 K using a Digilab FTS-40 Fourier transform infrared (FTIR) spectrometer with a maximum apodized resolution of 0.1 cm^{-1}. Laser excitation and fluorescence spectra were obtained using a 5 W. Coherent Innova 70 argon ion laser to optically pump a Spectra-Physics 375B dye laser. Rhodamine 560 dye dissolved in 100% ethyl-glycol was used as the lasing medium. The sample was cooled by a CTI-Cryogenics model 22C cold cycle refrigeration unit with temperature variability from 10 to 300 K provided by a Palm Beach Cryogenics temperature controller. Fluorescence was dispersed with a Spex Industries 500 M single monochromator. For fluorescence wavelengths in the range 400–800 nm, a Hamamatsu R9249 photomultiplier which was thermoelectrically cooled to −25 °C, was used to detect the light. For near-infrared light a liquid-nitrogen-cooled germanium detector was used with phase-sensitive detection provided by an Ortholoc model 9502 lock-in amplifier. Polarization spectra were recorded with a polaroid sheet with a Hanle wedge employed to correct for the differing response of the spectrometer to different polarizations. Corning glass filters were used to avoid second-order diffraction complicating spectra recorded in the 1000–1500 nm region. The lifetime of the higher-lying $^4G_{5/2}$ state was measured using a Laser Scientific model VSL-337 pulsed nitrogen laser to excite a Coumarin 500 dye laser. Data were collected using a Standford Research Systems SR430 multichannel analyzer.

The electron paramagnetic resonance measurements were made with a Bruker EMX10/12 *X*-band spectrometer (microwave frequency 9.644 GHz) with 100 kHz field modulation. The angular variation of the EPR spectra was measured by rotating the sample within the cavity. The measurements were performed under a microwave fluence of 0.5 mW and with a standard temperature of 5 K which was obtained with a continuous-gas-flow cryostat. The full range of the applied magnetic fields during an experiment was 0–1.5 T.

IV. POLARIZED LASER-EXCITED FLUORESCENCE SPECTROSCOPY

The $4f^5$ configuration, appropriate for trivalent Sm^{3+}, has 12 multiplets under 11 000 cm^{-1}: ^6H_J ($J=5/2,...,15/2$) and ^6F_J ($J=1/2,...,11/2$) as well as the excited states ^4G_J ($J=5/2,...,11/2$) and ^4F_J ($J=3/2,...,9/2$). The ground state is represented by $^6H_{5/2}$. For ^6H_J ($J=5/2,...,15/2$) and ^6F_J ($J=1/2,...,11/2$), there are 57 doubly degenerate crystal-field levels for Sm^{3+} ions with D_{2d} symmetry. For the $LiYF_4$ host, all of the Sm^{3+} ion energy levels have wave functions which necessarily transform as one of γ_6 and γ_7 irreducible representations of the D_{2d} double group as is appropriate for the point group symmetry of the Sm^{3+} ion site. The complete labeling scheme of Sm^{3+} crystal-field levels includes the parent $^{2S+1}L_J$ multiplet and the relevant irreducible representation (irrep). We adopt the common notation of a letter and a numerical subscript. Where it is known and appropriate, the irrep symmetry is also included. Thus the ground multiplet $^6H_{5/2}$ is labeled *Z*, with the ground state labeled $Z_1(\gamma_6)$, and the first excited multiplet is labeled *Y*, the second *X*, and so on (see Table II).

As the $^6H_{5/2}\rightarrow{}^4G_{5/2}$, $^4F_{3/2}$, and $^4G_{7/2}$ absorption transitions are nominally spin forbidden, no absorption spectra could be obtained for these multiplets with the 2-mm-thick $LiYF_4$:0.1% Sm^{3+} samples. These transitions are, however, weakly allowed as intermediate-coupling admixtures into both the $^6H_{5/2}$ and $^4G_{5/2}$ wave functions via the spin-orbit interaction break down the spin selection rule. Even so, for C_{4v} symmetry centers in Sm^{3+}-doped fluorite,[18] these transitions remain at less than 5% of the total transmission. To observe these absorption transitions, a $LiYF_4$:10% Sm^{3+} sample was studied. For crystals cooled to 10 K, all of the expected $J+1/2$ crystal-field states of the $^4G_{5/2}$, $^4F_{3/2}$, and $^4G_{7/2}$ multiplets could be identified as is indicated in Fig. 1. Employing the vastly enhanced sensitivity of laser excitation, the $^4G_{5/2}$ absorption features can be observed in the $LiYF_4$:0.1% Sm^{3+} sample (Fig. 2). To observe these transitions, the intensity of the fluorescence at 14 232 cm^{-1} was monitored using 3-mm-wide spectrometer slit widths. As in the absorption spectrum, three transitions are observed at fre-

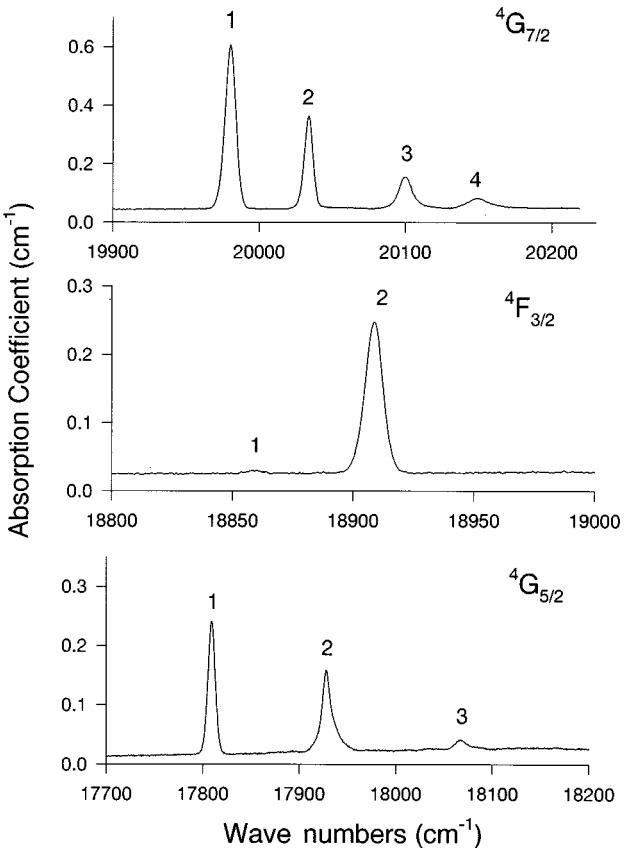

FIG. 1. 10 K absorption spectra for the $^4G_{5/2}$, $^4F_{3/2}$, and $^4G_{7/2}$ multiplets in $LiYF_4$:10% Sm^{3+}.

quencies of 17 810, 17 924, and 18 066 cm^{-1}, which are assigned as transitions to the three electronic energy levels of $^4G_{5/2}$ for the single Sm^{3+} ion center present in $LiYF_4$. The A_1 line at 17 810 cm^{-1} has no structure, while the A_2 and A_3 lines at 17 924 and 18 066 cm^{-1} are accompanied by structural lines with small intensities. These features are not caused by Sm^{3+} ion pairs or by a Sm^{3+} ion perturbed through vacancies or other impurities because the concentration (0.1%) of Sm^{3+} is very low and there is no structure for the A_1 line. Therefore, the additional features are attributable to phonon sideband absorption. The frequencies of the transitions and phonon energy are summarized in Table I. We have labeled these lines arbitrarily with lowercase letters. It is noted that the feature (labeled *e*) seen at an energy displacement of 218 cm^{-1} from the 17 810 cm^{-1} transition corresponds to a longitudinal optical phonon frequency of the host lattice.[19,20]

Sm^{3+} ion fluorescence has been studied both by argon ion excitation and by direct dye laser excitation of the $^4G_{5/2}$ multiplet itself. In neither case could emission from the excited $^4G_{7/2}$ or $^4F_{3/2}$ states be observed, and at 10 K, all fluorescence could be observed to emanate from the $^4G_{5/2}A_1(\gamma_7)$ state at 17 810 cm^{-1}. Fluorescence transitions to the lower-lying ^6H_J and ^6F_J multiplets are observed in the 17 800–7000 cm^{-1} region, and Fig. 3 presents fluorescence spectra with the static electric-field vector of the fluorescence polarized either perpendicular or parallel to the *c* axis. Of the 25 expected crystal-field components for the ^6H_J multiplets, only one could not be assigned. This is the $^6H_{13/2}V_7$ state which we have assigned from Fourier transform infrared absorption to be at an energy of 5173 cm^{-1}. In several cases, transitions which terminate on vibronic states of the host lattice have been observed as phonon sidebands. On the whole the observed vibronic intervals match those observed in excitation and these transitions have been labeled accordingly.

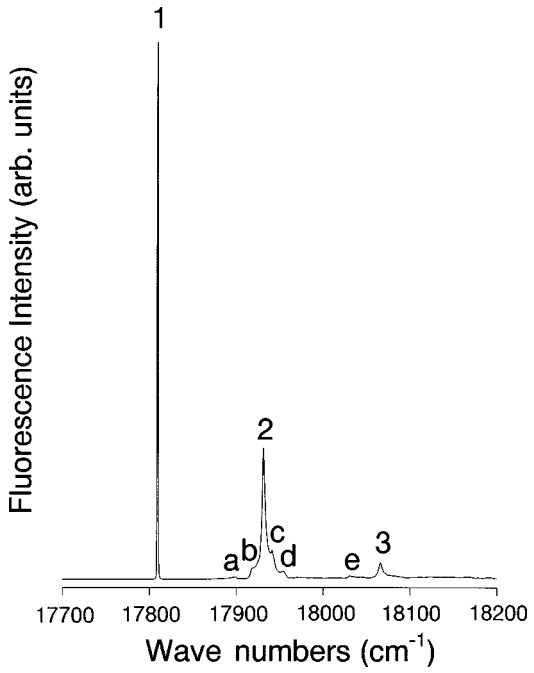

FIG. 2. 10 K laser excitation spectrum of the $^4G_{5/2}$ multiplet in $LiYF_4$:0.1% Sm^{3+}. Fluorescence was monitored at 14 232 cm^{-1} using 3 mm slits and neutral density filters.

Due to the proximity of the $^6H_{15/2}$, $^6F_{1/2}$, and $^6F_{3/2}$ multiplets, no experimental distinction can be made between the crystal-field splitting states of the three different multiplets. As a consequence, an arbitrary alphabetical label of *S* is given to the energy levels of these multiplets in Table II. This approach can be theoretically justified on the grounds that the wave functions of these states are considerably admixed by the crystal field. Not all of the expected transitions are observed, and this is attributed to the broader and partially overlapping higher-frequency states of these multiplets obscuring weaker transitions. Fluorescence transitions to the $^6F_{7/2}$ multiplet in the 9800–9700 cm^{-1} region are comparably weak and are superimposed upon a broad band of fluorescence which appears to be attributable to trace quantities

TABLE I. 10 K excitation transitions for the $^4G_{5/2}$ multiplet of $LiYF_4$:0.1% Sm^{3+}.

Label	Frequency	Shift from 17 810 cm^{-1}
A_1	17 810	0
a	17 897	87
b	17 915	105
A_2	17 924	114
c	17 934	127
d	17 948	138
e (LO)	18 028	218
A_3	18 066	256

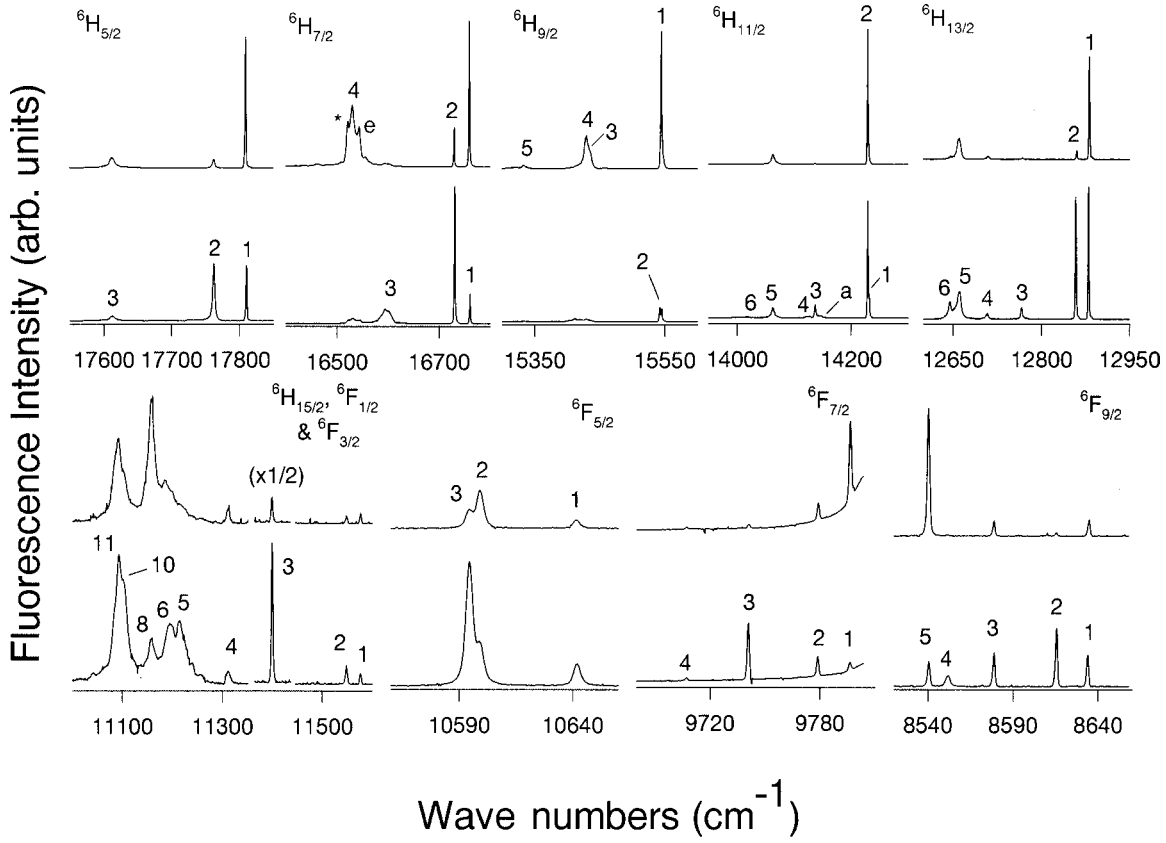

FIG. 3. 10 K polarized fluorescence spectra for the ${}^6H_J$ and ${}^6F_J$ multiplets. For each multiplet the upper spectrum is π polarized, while the lower spectrum is σ polarized. The $*$ notation indicates a transition which terminates on a vibronic state of the lattice and which has not been observed in excitation.

of YbF_3 (Ref. 21) in the SmF_3 used as a starting material.

All of the crystal-field splitting states of the ${}^6H_J$ and ${}^6F_J$ multiplets which have been inferred from the observed ${}^4G_{5/2}$ fluorescence have been confirmed by infrared absorption measurements. Good agreement between the laser excitation and IR absorption has been obtained.

V. FLUORESCENCE LIFETIME MEASUREMENTS

Excitation of either the ${}^4F_{3/2}$ multiplet at 18 900 cm^{-1} or the ${}^4G_{7/2}$ multiplet at 19 800 cm^{-1} yields fluorescence from the ${}^4G_{5/2}$ multiplet at 17 810 cm^{-1}. For pulsed laser excitation, a single exponential is observed when monitoring ${}^4G_{5/2}$ fluorescence. There is no rise time associated with the lifetime of the ${}^4F_{3/2}$ or ${}^4G_{7/2}$ multiplets. This indicates that the lifetimes of these higher-lying multiplets are predominantly governed by nonradiative relaxation, not measurable with the temporal resolution available here.

The fluorescence lifetime of the ${}^4G_{5/2}A_1(\gamma_7)$ state is measured to be 4.07 ± 0.05 ms at room temperature and 3.96 ± 0.05 ms at 10 K. Thus the ${}^4G_{5/2}$ lifetime is essentially static as the temperature of the sample is varied from room temperature to 10 K. This is not surprising as the energy gap between ${}^4G_{5/2}$ and the next-highest-energy multiplet (${}^6F_{11/2}$) is approximately 7500 cm^{-1}. To bridge such an energy gap with lattice phonons would require more than 12 phonons,[19,20] and such a process can be considered to make a negligible contribution to the ${}^4G_{5/2}$ lifetime, even at room temperature.

Given that the ${}^4G_{5/2}$ state is essentially metastable, the probability for the absorption of a second photon from that state should be reasonably high, giving rise to upconversion fluorescence by means of sequential absorption. Although such fluorescence was searched for, none could be detected for pump powers of up to 300 mW and at the limits of the detection capabilities available in this study. It is reasonable to assume that sequential absorption processes are occurring, but as the density of electronic states for the Sm^{3+} ion above 20 000 cm^{-1} is high, this optical excitation is quenched via nonradiative relaxation and all emission emanates from ${}^4G_{5/2}$.

VI. ELECTRON PARAMAGNETIC RESONANCE SPECTROSCOPY

The angular variations of the EPR spectra observed at 5 K with the magnetic field applied in the *ca* plane are shown in Fig. 4. The EPR spectrum consists of an intense single resonance line and several weak hyperfine lines due to isotopes ${}^{147}Sm$ and ${}^{149}Sm$ with the same nuclear spin $I=7/2$ and natural abundance 15.1% and 13.8%, respectively. Figure 5 shows the angular variation of the g values for those Sm^{3+} ions with zero nuclear spin. Although the spectrum with the magnetic field applied parallel to the c axis was not observed in the range of 0–1.5 T, we can infer values of $g_\parallel$ and $g_\perp$ of 0.410 ± 0.005 and 0.644 ± 0.002, respectively, from the angular variation that is apparent.

The resonance line is split into eight lines due to the hy-

TABLE II. Experimental and calculated crystal-field levels for the ^6H_J, ^6F_J, $^4G_{5/2}$, $^4F_{3/2}$, and $^4G_{7/2}$ multiplets under D_{2d} symmetry in $LiYF_4:Sm^{3+}$. The experimental state energies are in wave numbers (as measured in air, ± 1).

Multiplet	State	Symmetry	Calculated	Experimental	Multiplet	State	Symmetry	Calculated	Experimental
$^6H_{5/2}$	Z_1	γ_6	7.2	0		S_5	γ_7	6596.6	6597
	Z_2	γ_7	60.5	51		S_6	γ_6	6604.0	6617
	Z_3	γ_7	208.9	198		S_7	γ_7	6616.0	—
$^6H_{7/2}$	Y_1	γ_6	1044.7	1051		S_8	γ_6	6647.8	6652
	Y_2	γ_7	1070.3	1079		S_9	γ_7	6673.5	—
	Y_3	γ_7	1207.4	1216		S_{10}	γ_7	6719.7	6709
	Y_4	γ_6	1269.0	1279		S_{11}	γ_6	6720.4	6718
$^6H_{9/2}$	X_1	γ_7	2259.1	2268	$^6F_{5/2}$	Q_1	γ_7	7155.6	7169
	X_2	γ_6	2261.1	2271		Q_2	γ_6	7211.1	7211
	X_3	γ_6	2376.0	2375		Q_3	γ_7	7223.5	7216
	X_4	γ_7	2389.7	2381	$^6F_{7/2}$	R_1	γ_6	8009.5	8013
	X_5	γ_6	2473.3	2477		R_2	γ_7	8021.1	8031
$^6H_{11/2}$	W_1	γ_7	3571.9	3578		R_3	γ_7	8061.4	8069
	W_2	γ_6	3580.6	3579		R_3	γ_6	8113.2	8103
	W_3	γ_7	3665.2	3673	$^6F_{9/2}$	P_1	γ_7	9181.5	9176
	W_4	γ_6	3680.8	3683		P_2	γ_6	9190.2	9195
	W_5	γ_6	3747.3	3747		P_3	γ_6	9227.1	9233
	W_6	γ_7	3795.7	3790		P_4	γ_7	9259.9	9258
$^6H_{13/2}$	V_1	γ_6	4934.5	4929		P_5	γ_6	9265.0	9270
	V_2	γ_7	4954.5	4951	$^4G_{5/2}$	A_1	γ_7	17 797.2	17 810
	V_3	γ_7	5042.4	5044		A_2	γ_6	17 937.7	17 924
	V_4	γ_6	5102.7	5102		A_3	γ_7	18 079.8	18 066
	V_5	γ_6	5152.8	5151	$^4F_{3/2}$	B_1	γ_6	18 881.4	18 860
	V_6	γ_7	5156.2	5164		B_2	γ_7	18 890.4	18 909
	V_7	γ_7	5170.8	5173	$^4G_{7/2}$	C_1	γ_7	19 952.9	19 982
$^6H_{15/2}$,	S_1	γ_7	6246.9	6236		C_2	γ_6	20 032.7	20 034
$^6F_{1/2}$, $^6F_{3/2}$	S_2	γ_6	6275.5	6263		C_3	γ_7	20 097.3	20 100
	S_3	γ_6	6429.3	6416		C_4	γ_6	20 165.3	20 151
	S_4	γ_6	6515.8	6503					

perfine interaction between the effective electron spin of $S=1/2$ and the nuclear spin of $I=7/2$. The spectrum shows an unequal spacing in the hyperfine structure; that is, there is an increasing separation between each adjacent hyperfine line as the resonance field increases. The central field, being equal to the average field of the hyperfine lines due to $M_I=-1/2$ and 1/2, is slightly shifted to a lower field, compared with that of the intense line with $I=0$. This effect can be explained by the second-order perturbation given by Bleaney.[22,23] Calculation of the field positions using this correction gives the parameters $A_\parallel=205\pm5$ MHz and $A_\perp=735\pm5$ MHz for ^{147}Sm and $A_\parallel=165\pm5$ MHz and $A_\perp=605\pm5$ MHz for ^{149}Sm. The ratio of $A_\parallel$ for ^{147}Sm to that for ^{149}Sm is 1.24, in exact agreement with the ratio of the respective magnetic moments.

VII. D_{2d} SYMMETRY CRYSTAL-FIELD ANALYSIS

The f^5 configuration consists of 1001 twofold degenerate electronic states. In order to obtain a physically realistic approximation to the entire configuration, the basis set for the crystal-field calculations have been truncated to the lowest 30 free-ion multiplets. The calculations, which were performed using the *f*-shell empirical crystal-field fitting routines of Mike Reid of the University of Canterbury, New Zealand, used the $LiYF_4:Eu^{3+}$ optimized crystal-field parameters of Görller-Walrand *et al.*[5] as a starting point. The free-ion Hamiltonian has been parametrized as

$$H_{\rm cf}=\sum_{k=2,4,6}F^k f_k+\sum_i \zeta \mathbf{l}_i\cdot\mathbf{s}_i+\alpha L(L+1)+\beta G(G_2)+\gamma G(R_7)+\sum_{h=0,2,4}M^h m_h+\sum_{k=2,4,6}P^k p_k+\sum_{i=2,3,4,6,7,8}T^i t_i. \quad (1)$$

The predominant terms in this Hamiltonian are the electrostatic and spin-orbit interactions represented by parameters F^k and ζ, which are varied in the fit. The remaining terms represent smaller interactions, which nevertheless play an important role in the accurate description of the energy level structure of rare-earth ions. These are the configuration interactions (α,β,γ), spin-spin, and spin-other-orbit interactions, represented by the parameters M^h, the two-body electrostatically correlated magnetic interactions, with parameters P^k, and the three-particle configuration interactions T^i. These are not varied at all, but rather are held constant at the values given in Ref. 24.

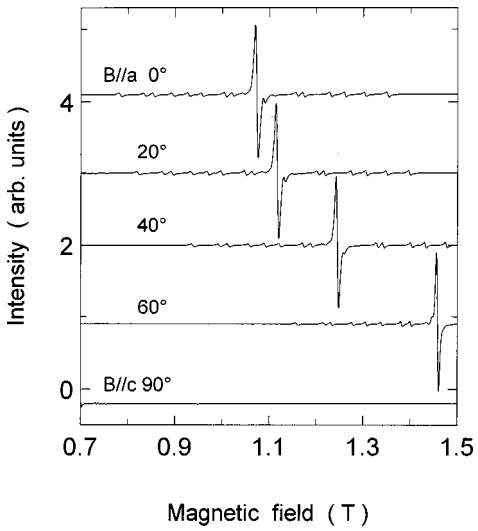

FIG. 4. Angular variation of the EPR spectra of Sm^{3+} in $LiYF_4$ observed at 5 K with the magnetic field applied in the *ca* plane.

In this study, we fit the experimental energy eigenvalues to a parametric Hamiltonian which is appropriate for D_{2d} symmetry. This can be written as

$$H_{\mathrm{cf}}=B_0^2C_0^{(2)}+B_0^4C_0^{(4)}+B_0^6C_0^{(6)}+B_4^4(C_4^{(4)}+C_{-4}^{(4)}) +B_4^6(C_4^{(6)}+C_{-4}^{(6)}). \quad (2)$$

Fifty-five levels of the Sm^{3+} ion center in $LiYF_4$:Sm^{3+} were fitted to nine free parameters excluding the average energy. Table II presents the experimental and calculated energy levels with good agreement obtained having a standard deviation of 10.7 cm^{-1}. Table III shows the optimized parameters of the fit. The crystal-field parameter values shown in parentheses are the appropriate optimized parameters for $LiYF_4$:Eu^{3+}. As can be seen, good agreement is obtained between the two, giving confidence in the fit obtained here. Fitting to the measured experimental data assuming S_4 symmetry yields optimized values of the imaginary components

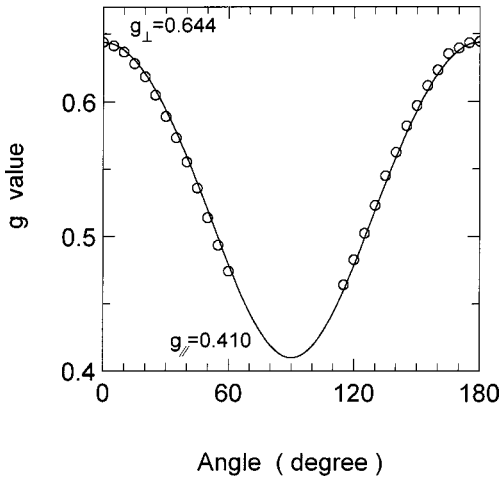

FIG. 5. Angular variation of the *g* values in the *ca* plane.

TABLE III. Optimized free-ion and D_{2d} symmetry crystal-field parameters for $LiYF_4$:Sm^{3+}. All quantities are in wave numbers except *n*, the number of data points. The values in square brackets have not been varied.

Parameter	Sm^{3+}	Eu^{3+} [a]
F^2	79 533	
F^4	56 768	
F^6	40 087	
α	[20.16]	
β	[−566.9]	
γ	[1500]	
T^2	[300]	
T^3	[36]	
T^4	[56]	
T^6	[−347]	
T^7	[373]	
T^8	[348]	
M^{tot}	[2.60]	
P^{tot}	[357.0]	
ζ	1170	
B_0^2	368	349
B_0^4	−755	−749
B_4^4	−938	−1054
B_0^6	−64	−93
B_4^6	−898	−778
σ	10.7	
n	55	

[a]Reference 5.

of B_4^4 and B_4^6 which are negligible. As a consequence, the effects of any low-symmetry distortion are not included in this analysis.

In order to calculate the magnetic splitting factors of the ground state, the Zeeman interaction term

$$H_{\mathrm{Zeeman}}=\mu_B g_L(\mathbf{L}+2\mathbf{S})\cdot\mathbf{B} \quad (3)$$

was included in the Hamiltonian and the combined crystal-field and Zeeman matrices were simultaneously diagonalized. From this, the ground-state magnetic splitting factors are calculated as $g=\Delta E/\mu_B B$, where ΔE is the separation of the Zeeman split ground levels, B is the magnitude of the applied magnetic field, and g_L is the Landé g factor corrected for the effects of intermediate coupling. This yields magnetic splitting factors for the $Sm^{3+}Z_1(\gamma_6)$ ground state of $g_\parallel=0.450$ and $g_\perp=0.728$, in good agreement with the EPR values of $g_\parallel=0.410\pm0.005$ and $g_\perp=0.644\pm0.002$.

VIII. CONCLUSIONS

We have reported upon the spectroscopy of $LiYF_4$:Sm^{3+} using optical absorption, laser excitation and fluorescence, and EPR. We have confirmed the tetragonal symmetry of the Sm^{3+} center and determined 55 of its crystal-field energy eigenvalues and their irrep symmetries under D_{2d} point group symmetry. EPR has measured the values of the *g* tensors parallel and perpendicular to the fourfold axis of the

center to be $g_{\parallel}=0.410\pm0.005$ and $g_{\perp}=0.644\pm0.002$; these are very similar to the values measured for Sm^{3+} doped into calcium tungstate with the same scheelite structure.[25] A full description of the EPR spectrum of Sm^{3+} in $LiYF_4$ requires that electron-nuclear effects be taken into account for the ^{147}Sm and ^{149}Sm isotopes with nonzero nuclear spin. For the ^{147}Sm isotope magnetic hyperfine constants of $A_{\parallel}=205\pm5$ MHz and $A_{\perp}=735\pm5$ MHz are determined, while for the ^{149}Sm isotope they are $A_{\parallel}=165\pm5$ MHz and $A_{\perp}=605\pm5$ MHz. A crystal-field analysis for the 55 experimental crystal-field energy levels gives good account of the experimental data assuming D_{2d} symmetry. The calculated crystal-field wave functions yield ground-state magnetic splitting factors in close agreement with the measured g factors.

ACKNOWLEDGMENTS

This work was funded by the Engineering and Physical Sciences Research Council of the United Kingdom under Research Contract No. GR/K/8802. Additional support has been provided by the Royal Society and British Council. The authors wish to thank Dr. Mike F. Reid for kindly providing his crystal-field fitting routines and for assistance and instruction on their use, and Dr. G. D. Jones and Dr. R. J. Reeves of the University of Canterbury, New Zealand, for allowing access to their Digilab FTIR spectrometer for measuring the ^6H_J and ^6F_J infrared absorption transitions. Technical assistance has been provided by D. Clark and R. G. Dawson who oriented, cut, and polished the samples used for spectroscopy.

[1] M. Tonelli, M. Falconieri, A. Lanzi, G. Salvetti, and A. Toncelli, Opt. Commun. **129**, 62 (1996).
[2] L. Esterowitz, F. J. Bartoli, R. E. Allen, D. E. Wortman, C. A. Morrison, and R. P. Leavitt, Phys. Rev. B **19**, 6442 (1979).
[3] C. Görller-Walrand, M. Behets, P. Porcher, O. K. Moune-Minn, and I. Laursen, Inorg. Chim. Acta **109**, 83 (1985).
[4] B. Bipin, K. K. Sharma, and L. E. Erickson, J. Phys.: Condens. Matter **2**, 5703 (1990).
[5] C. Görller-Walrand, K. Binnemans, and L. Fluyt, J. Phys.: Condens. Matter **5**, 8359 (1993).
[6] L. Fluyt, K. Binnimans, and C. Görller-Walrand, J. Alloys Compd. **225**, 71 (1995).
[7] M. Malinowski, M. F. Joubert, and B. Jacquier, Phys. Rev. B **50**, 12 367 (1994).
[8] M. Malinowski, M. F. Joubert, and B. Jacquier, J. Lumin. **60&61**, 179 (1994).
[9] A. W. Kueny, W. E. Case, and M. E. Koch, J. Opt. Soc. Am. B **10**, 1834 (1993).
[10] T. Danger, J. Koetke, R. Brede, E. Heumann, G. Huber, and B. H. T. Chai, J. Appl. Phys. **76**, 1413 (1994).
[11] W. Lenth and R. M. Macfarlane, J. Lumin. **45**, 346 (1990).
[12] T. Hebert, R. Wannemacher, R. M. Macfarlane, and W. Lenth, Appl. Phys. Lett. **60**, 2592 (1992).
[13] J. R. O'Connor and H. A. Bostick, J. Appl. Phys. **33**, 1868 (1962).
[14] M. J. Treadway and R. C. Powell, Phys. Rev. B **11**, 862 (1975).
[15] T. Luxbacher, H. P. Fritzer, and C. D. Flint, J. Phys.: Condens. Matter **7**, 9683 (1995).
[16] G. Blasse, in *Spectroscopy of Solid State Laser Type Materials*, edited by B. Di Bartolo (Plenum, New York, 1987).
[17] W. A. Shand, J. Cryst. Growth **5**, 143 (1969).
[18] J.-P. R. Wells and R. J. Reeves (unpublished).
[19] S. Salaün, M. T. Foroni, A. Bulou, M. Rousseau, P. Simon, and J. Y. Gesland, J. Phys.: Condens. Matter **9**, 6941 (1997).
[20] S. Salaün, A. Bulou, M. Rousseau, B. Hennion, and J. Y. Gesland, J. Phys.: Condens. Matter **9**, 6957 (1997).
[21] N. Uehara, K. Ueda, and Y. Kubota, Jpn. J. Appl. Phys., Part 1 **35**, L499 (1996).
[22] B. Bleaney, Philos. Mag. **42**, 441 (1951).
[23] J. R. Pilbrow, *Transition Ion Electron Paramagnetic Resonance* (Clarendon, Oxford, 1990), p. 610.
[24] W. T. Carnall, G. L. Goodman, K. Rajnak, and R. S. Rana, J. Chem. Phys. **90**, 3443 (1989).
[25] J. Kirton, Phys. Lett. **16**, 209 (1965).